Institutional Repository - Research Portal
Dépôt Institutionnel - Portail de la Recherche
researchportal.unamur.be
University of Namur

RESEARCH OUTPUTS / RÉSULTATS DE RECHERCHE

Random walk on temporal networks with lasting edges

Petit, Julien; Gueuning, Martin; Carletti, Timoteo; Lauwens, Ben; Lambiotte, Renaud

Published in:
Physical review. E

DOI:
10.1103/PhysRevE.98.052307

Publication date:
2018

Document Version
Publisher's PDF, also known as Version of record

Link to publication

Citation for pulished version (HARVARD):
Petit, J, Gueuning, M, Carletti, T, Lauwens, B & Lambiotte, R 2018, 'Random walk on temporal networks with lasting edges', *Physical review. E*, vol. 98, no. 5, 052307. https://doi.org/10.1103/PhysRevE.98.052307

General rights
Copyright and moral rights for the publications made accessible in the public portal are retained by the authors and/or other copyright owners and it is a condition of accessing publications that users recognise and abide by the legal requirements associated with these rights.

- Users may download and print one copy of any publication from the public portal for the purpose of private study or research.
- You may not further distribute the material or use it for any profit-making activity or commercial gain
- You may freely distribute the URL identifying the publication in the public portal ?

Take down policy
If you believe that this document breaches copyright please contact us providing details, and we will remove access to the work immediately and investigate your claim.

Download date: 03. Jul. 2025

Random walk on temporal networks with lasting edges

Julien Petit,[1,2,*] Martin Gueuning,[2,3] Timoteo Carletti,[2] Ben Lauwens,[1] and Renaud Lambiotte[4]
[1]*Mathematics Department, Royal Military Academy, Brussels, Belgium*
[2]*naXys, Namur Institute for Complex Systems, Namur, Belgium*
[3]*ICTEAM, Université Catholique de Louvain, Louvain-la-Neuve, Belgium*
[4]*Mathematical Institute, University of Oxford, Oxford, United Kingdom*

(Received 10 September 2018; published 20 November 2018)

We consider random walks on dynamical networks where edges appear and disappear during finite time intervals. The process is grounded on three independent stochastic processes determining the walker's waiting time, the up time, and the down time of the edges. We first propose a comprehensive analytical and numerical treatment on directed acyclic graphs. Once cycles are allowed in the network, non-Markovian trajectories may emerge, remarkably even if the walker and the evolution of the network edges are governed by memoryless Poisson processes. We then introduce a general analytical framework to characterize such non-Markovian walks and validate our findings with numerical simulations.

DOI: 10.1103/PhysRevE.98.052307

I. INTRODUCTION

Random walks play a central role in different fields of science [1–3]. Despite the apparent simplicity of the process, the study of random walks remains an active domain of research [4–8]. Within the field of network science, a central theme focuses on the relation between patterns of diffusion and network structure [9]. Important applications include the design of centrality measures based on the density of walkers on the nodes [10], or community detection methods looking for regions of the network where a walker remains trapped for long times [11–13]. The mathematical properties of random walks on static networks are overall well established [14], and essentially equivalent to those of a Markov chain. However, the process becomes much more challenging when the network is itself a dynamical entity, with edges appearing and disappearing in the course of time [15–17]. The temporal properties of networks have been observed and studied in a variety of empirical systems, and their impact on diffusive processes explored by means of numerical simulations [18–20] and analytical tools [21].

Mathematical analysis of dynamics on temporal networks often relies on the assumption that links activate during an infinitesimal duration [22]. In the case of random walks, this framework naturally reduces to standard continuous-time random walks on static, weighted networks. Even in this simplified case, however, the dynamics exhibits interesting properties including the so-called waiting-time paradox. When the dynamics of the edges is Poissonian, trajectories are encoded by a Markov chain, whereas the timings obtained from a non-Poisson renewal process lead to nontrivial properties such as the emergence of non-Markovian trajectories. In that case the trajectory of the walker generally depends on its previous jumps and not only on its current location [23,24]. The emergence of non-Markovian trajectories is even more pronounced in situations when the activations of the edges are correlated, often requiring the use of higher-order models for the data [25,26]. However, this whole stream of research neglects an important aspect of the edge dynamics: the nonzero duration of their availability, which has been observed and characterized in a variety of real-life systems, including sensor data [27–29]. The finite duration of edges availability has important practical implications, including in community detection [30]. Theoretically, some results have been obtained within the framework of switching systems, e.g., by replacing the constant Laplacian matrix L by a time-dependent one $L(t)$ for the diffusion [31–33], but a master equation approach derived from a microscopic model of the dynamics is, to the best of our knowledge, still lacking.

Our main objective is to develop an analytical framework for random walks on temporal networks with finite up times. Given a network of potential connections between a fixed set of nodes, the model is defined by three temporal processes. Each process comes with its own time scale, associated to the motion of the random walker, the time between two successive active time spans of the edges, and the duration of these time spans. In contrast with previous research, we derive a master equation from the model specifications, without implicitly assuming memoryless dynamics for the walker, and consider the resulting trajectories of the random walker [34]. The competition between three time scales makes the problem particularly rich and we show how certain master equations already known in the literature are recovered in limit regimes. Indeed, the next section makes clear that our framework is quite general, and therefore it can describe the regular single time-scale continuous-time random walks on networks, the so-called active node-centric and passive edge-centric models. In the first case, the trajectory of the walker is solely determined by the waiting time on the nodes, since the edges are always active. In the second case, the time spans between two instantaneous up times of the edges determine the dynamics, as the walker is always ready to jump. But generally speaking, not only one time scale prevails and neither of the former two asymptotic regimes can capture

*julien.petit@unamur.be

 ©2018 American Physical Society

the full dynamics, thereby establishing the need to study the implications of three competing time scales.

This paper is organized as follows. In Sec. II, we describe the model and its parameters. In Sec. III, we derive a master equation for the density of the walker valid for directed acyclic graphs (DAGs). Particular cases for the model parameters and their ensuing dynamics are discussed. These equations are revisited in Sec. IV, where we consider the impact of cycles in the graph on the Markovianity of the process. The analytical predictions are confronted with numerical simulations throughout this work. Section V gives more details about the numerical implementation of our formalism. We finally conclude and give perspectives in Sec. VI.

II. MODEL

Let V be a fixed set of N nodes and E be a set of directed edges between these nodes. We denote by $\mathcal{G} = (V, E)$ the static graph determining which edges are available in the dynamic graph with time-dependent adjacency matrix $A(t)$. The dynamic graph can assume any of the $2^{|E|}$ possible configurations allowed by $\mathcal{G}$. In our model-driven approach, each edge $(i, j) = i \to j \in E$ is characterized by the following:

(i) a down-time probability density function (PDF) $D_{ij}(t)$, $t \in \mathbb{R}^+$, which determines for how long the edge remains inactive;

(ii) an up-time PDF $U_{ij}(t)$, $t \in \mathbb{R}^+$, which rules the duration that the edge is available to the walker.

In this work, the random variables associated with the densities U_{ij} and D_{ij} are assumed to have finite expectation. The adjacency matrix can be written as

$$A(t) = \sum_{i \in \mathbb{Z}} G_i \mathbb{1}_{\{t_i \leqslant t < t_{i+1}\}}(t) \tag{1}$$

with $\cdots < t_{-1} < t_0 \leqslant 0 < t_1 < \cdots$ the successive times of the rewiring, and G_i a fixed adjacency matrix (Fig. 1). Let $k_i^{\text{in}}(t) = \sum_{j=1}^{N} A_{ji}(t)$ be the in degree of node i at time t, and $k_i^{\text{out}}(t) = \sum_{j=1}^{N} A_{ij}(t)$ be the out degree. We define the set of nodes reachable from i in the underlying graph $V_i = \{j \in V \mid i \to j \in E\}$, and $|V_i|$ its cardinality, namely the out

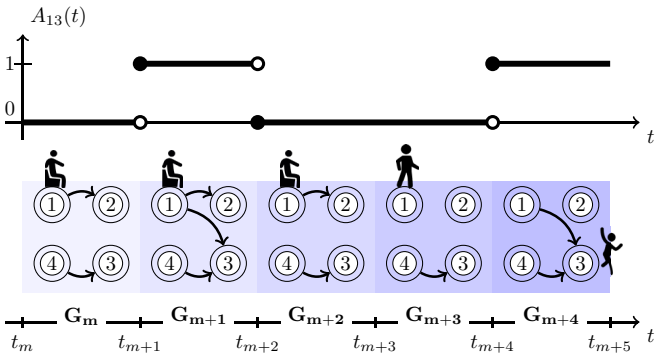

FIG. 1. Directed temporal network with four nodes (below) and the (1,3) entry of the time-dependent adjacency matrix $A(t)$ (above). Note that $A(t)$ is right continuous and is given by $A(t) = G_i$ for $t_i \leqslant t < t_{i+1}$. In this example, the up time $t_{m+2} - t_{m+1}$ of edge $1 \to 3$ follows the density $U_{13}(t)$, while the down time $t_{m+4} - t_{m+2}$ has density $D_{13}(t)$. At every random rewiring time t_i, almost surely only one edge changes states.

degree of node i in $\mathcal{G}$. Similarly, $V_i' = \{j \in V \mid j \to i \in E\}$ and $|V_i'|$ results to be the in degree of node i. We make the assumption that there are no isolated nodes in $\mathcal{G}$: for every $i \in E$, $\max\{|V_i|, |V_i'|\} > 0$.

Let us define the random walk. A continuous-time random walk on a dynamical graph with adjacency matrix $A(t)$, $t \in \mathbb{R}$, is a process $\{A(t), i_W(t)\}$ where $i_W(t) \in V$ is the node occupied by the walker at time t. Upon arrival on a node i, the walker is assigned a waiting time according to the PDF $\psi_i(t)$ which generally depends on the node (see Fig. 2, first, second, and third cartoon from the left). After the waiting time has elapsed, the walker selects one of the available leaving edges uniformly, namely with probability $1/k_i^{\text{out}}(t)$. If no edge is available, the walker is trapped on the node (Fig. 2, fourth cartoon) and waits for the first leaving edge to appear to perform the jump (Fig. 2, fifth cartoon). Note that in the latter case, almost surely there is no choice to be made: no two or more edges can activate at the same time.

Let us observe that a possible variant of this random walk could consist of assigning a new waiting-time according to ψ_i for the walker trapped on a node because of the lack of available edges once it is ready to jump. This process was studied in [34], where the authors exclusively focus on the asymptotic state of the process.

Our model is an extension of the standard active node-centric and passive edge-centric random walks in temporal networks [17], where edge duration is instantaneous. In the former, the motion is determined by the waiting time of the walker and, once a jump takes place, all the edges in $\mathcal{G}$ are available—or at least the ones exiting from the node where the walker is located. In the latter case, the walker is ready to jump as soon as it arrives on a new node, and it takes the first edge that appears—the walker thus passively follows the appearing edges modeled by a renewal process. These two cases correspond to asymptotic regimes described by our model when a time scale dominates over the others. In general, however, the process is determined by the competition of three time scales. Figure 2 summarizes possible scenarios labeled from A to D corresponding to the four distinct cases, where the dynamics of the down and up times are either significantly shorter or significantly longer than the characteristic waiting time of the walker. At the right border of the domain, in the region ranging from B to C, when the walker is ready to jump, the possible extra waiting time for an edge to become available is usually short, and the network dynamics can be neglected. Therefore, the node-centric random walk is a good proxy for our model. In the region centered around D, the same type of analysis leads instead to neglecting the waiting time of the walker. In general however, as in the center of the domain, in the area between the dotted regions, neither the walker nor the edge's dynamics can be neglected. This region is the focus of our work.

III. CASE OF DIRECTED ACYCLIC GRAPHS

As a first step, we consider the trajectory of a walker performing a random walk as defined above on a directed acyclic graph (DAG). The reason for that is twofold:

(1) DAGs include directed trees and find many applications; see for instance [35]. Every undirected graph possesses

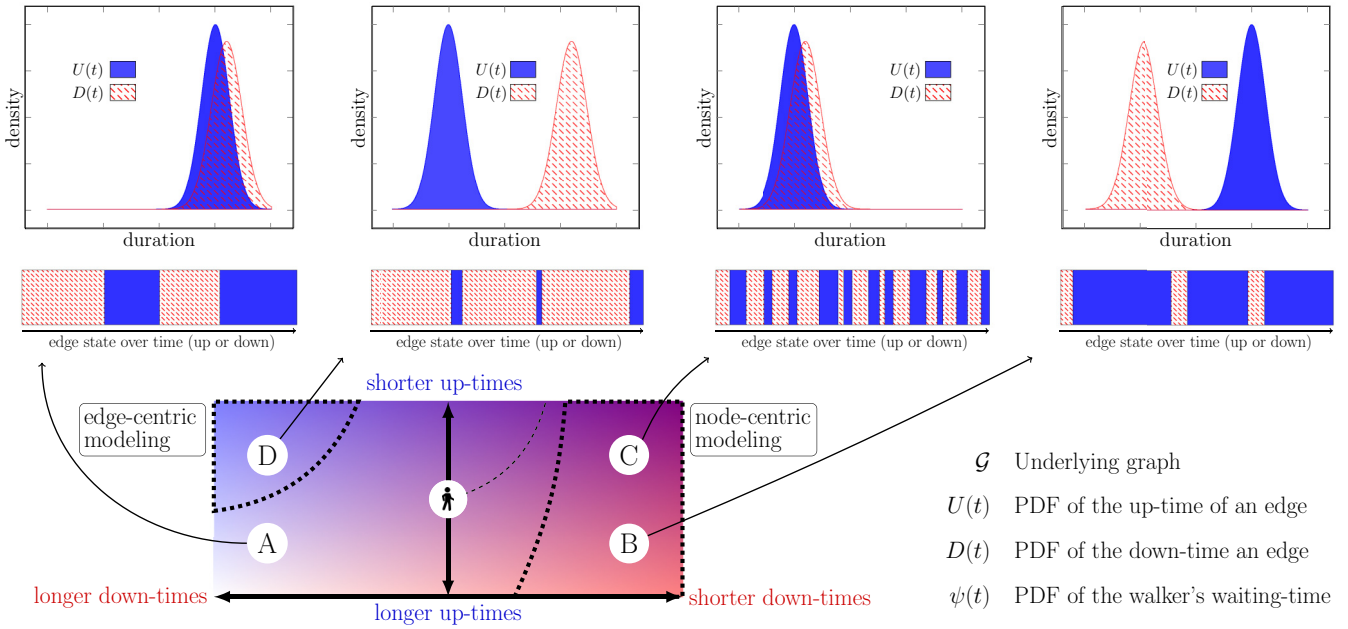

FIG. 2. Three time scales are present in the model: One governs the rest state of the walker in the nodes and two associated with the duration of the up times and down times of the edges. The overall dynamics will depend on the relative weights of such time scales, as we schematically report here. The bottom panel represents the up-time and down-time durations of the edges with respect to the walker's self-imposed waiting time upon arrival on a node. The four corners identified by the letters $A-D$ represent the cases where the time scale for the edge's dynamics is clearly separated from that of the walker (hereby located in the center of the domain of the bottom panel, and schematically represented by a standing icon). Each of these four situations is described by one of the four top panels, representing typical up-time and down-time probability density functions (PDF's) $U(t)$ and $D(t)$, which complement the walker's possibly node-dependent PDF $\psi(t)$ as the three dynamical parameters of the model. The rectangles with the red and blue bars show representative realizations of the stochastic processes of edge active and inactive time spans according to the densities reported above. The blue shaded (respectively red hatched) rectangles stand for periods of edge availability (respectively unavailability). The proposed model depends on the four parameters in the bottom right panel. It is general enough to tackle also the situations where there is no sharp time-scale separation, and none of the dynamics is extreme enough to be neglected, as in the region bounded by the dashed lines in the bottom panel.

an acyclic orientation. Moreover, by contracting each strongly connected component, every directed graph can be mapped to a DAG. Figure 3 illustrates that process. The material presented in this section therefore provides tools to analyze a random walk on a coarse-grained model obtained by condensation of a given graph into a DAG.

(2) As we will show next, the presence of cycles in the graph will remove the Markov property from the random walk. Hence, the analysis of our model on a DAG will serve, in a second step, as a limiting case on which to consider more general organizations. The approximation using DAGs is expected to be good when edges along a path can be considered statistically independent. The conditions for this to hold will be discussed further in Sec. IV.

As will become clear (see Sec. III E), the model on DAGs can be viewed as a one-density, node-centric (or edge-centric) random walk.

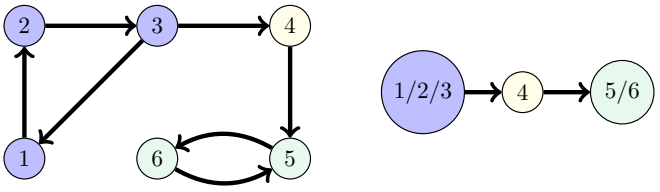

FIG. 3. Mapping of a directed network with cycles (a) to a DAG (b) through a condensation process. Strongly connected components are transformed into supernodes.

A. Master equation on a DAG

The notations in this section are adapted from [22]. Let $n_i(t)$ be the probability for the walker to be on node i at time t,

$$n_i(t) = P\{i_W(t) = i\}. \tag{2}$$

If $q_i(t)$ is the PDF of the arrival time on node i, and $\Phi_i(t,\tau)$ is the probability to stay on node i on the interval $[\tau, t]$ with τ the arrival time on node i, then

$$n_i(t) = \int_0^t q_i(\tau)\Phi_i(t,\tau)d\tau. \tag{3}$$

Let $T_{ji}(t,\tau)$ be the PDF of the transition time from node i to j, with τ the arrival time on node i. Let also $T_{\bullet i}(t,\tau)$ denote

the PDF of the time of the jump from node i. We have

$$\Phi_i(t,\tau) = 1 - \int_\tau^t T_{\bullet i}(\nu,\tau)d\nu = 1 - \int_\tau^t \sum_{j\in V_i} T_{ji}(\nu,\tau)d\nu. \quad (4)$$

We want to write the column vector $\mathbf{n}(t) = (n_1(t),\dots,n_N(t))^T$ in terms of the transition density T_{ij} and of the initial condition $\mathbf{n}(0)$. Looking at (3) and (4), we search for an appropriate expression for $q_i(t)$. Let $q_i^{(k)}(t)$ be the probability to arrive on node i at time t in exactly $k \in \mathbb{N}$ jumps. Then we have

$$q_i(t) = \sum_{k=0}^{\infty} q_i^{(k)}(t) = \sum_{k\geqslant 1} q_i^{(k)}(t) + q_i^{(0)}(t), \quad (5)$$

with initial condition $q_i^{(0)}(t) = n_i(0)\delta(t)$. Equivalently,

$$q_i(t) = \sum_{k=0}^{\infty} q_i^{(k+1)}(t) + q_i^{(0)}(t), \quad (6)$$

where

$$q_i^{(k+1)}(t) = \sum_j \int_0^t q_j^{(k)}(\nu)T_{ij}(t,\nu)d\nu. \quad (7)$$

Summing on both sides over $k \geqslant 0$ and adding $q_i^{(0)}(t)$ yields

$$q_i(t) = \sum_j \int_0^t q_j(\nu)T_{ij}(t,\nu)d\nu + q_i^{(0)}(t). \quad (8)$$

In vector form, with $\mathbf{q}(t) = (q_1(t),\dots,q_N(t))^T$, we have

$$\mathbf{q}(t) = \mathcal{T}\mathbf{q}(t) + \mathbf{q}^{(0)}(t), \quad (9)$$

where $\mathcal{T}$ is the linear integral operator acting on $\mathbf{q}(t)$ defined by

$$\mathcal{T}\mathbf{q}(t) = \int_0^t T(t,\nu)\mathbf{q}(\nu)d\nu, \quad i = 1,\dots,N, \quad (10)$$

where $T(t,\nu)$ is a matrix function with component (i,j) given by $T_{ij}(t,\nu)$. Due to the acyclic nature of the graph and as will become clear after remark 3 at the end of Sec. III C, the transition density actually only depends on the duration $t-\tau$. As a result, Eq. (10) is a convolution and applying a Laplace transform allows us to solve (9) for $\mathbf{q}(t)$, as was done in Ref. [22].

Once $\mathbf{q}(t)$ is found, we consider Eq. (3), which can be cast under the form

$$\mathbf{n}(t) = \mathcal{P}\mathbf{q}(t), \quad (11)$$

where operator $\mathcal{P}$ is diagonal and given by

$$[\mathcal{P}\mathbf{q}(t)]_i = \int_0^t \Phi_i(t,\tau)q_i(\tau)d\tau, \quad i = 1,\dots,N. \quad (12)$$

Observe that this is again a convolution, because $\Phi_i(t,\tau)$ is essentially $\Phi_i(t-\tau)$. The right-hand side of (12) can be computed directly in the time domain, or through a Laplace transform. In the latter case we obtain for each component $\hat{n}_i(s) := \int_0^\infty n_i(t)e^{-st}dt$ a product in the Laplace domain, and we ultimately find $\mathbf{n}(t) = (n_1(t),\dots,n_N(t))$ as a function of the initial density $\mathbf{n}(0)$ by computing the inverse transform of these products.

B. On the use of the Laplace transform in the case of a DAG

It is not mandatory to use the Laplace transform to solve the integral equations for $\mathbf{q}(t)$ and then get $\mathbf{n}(t)$. We can proceed directly in the time domain and solve the equation relying on the acyclic nature of the graph. We detail this alternative approach, which does not rely on the convolution structure of the integral equations.

Remark 1. This method also applies when we drop the acyclic assumption on $\mathcal{G}$ in Sec. IV and we have to solve Eq. (50).

Let us first recall Neumann's Lemma.

Theorem 1. Let $\mathcal{T}$ be a linear bounded operator on a Banach space X. If $||\mathcal{T}|| = \sup_{||x||\leqslant 1} ||\mathcal{T}x|| < 1$, then $I-\mathcal{T}$ is invertible and is given by the Neumann series

$$(I-\mathcal{T})^{-1} = \sum_{k=0}^{\infty} \mathcal{T}^k = I + \mathcal{T} + \mathcal{T}^2 + \cdots.$$

The theorem is applicable for this convolution-type linear Volterra integral equation with square integrable convolution kernels (see [36] Theorem 3.7.7, p. 77), and Eq. (9) gives

$$\mathbf{q}(t) = (I-\mathcal{T})^{-1}\mathbf{q}^{(0)}(t) = \sum_{k=0}^{\infty} \mathcal{T}^k\mathbf{q}^{(0)}(t) \quad (13)$$

$$= \sum_{k=0}^{\infty} \mathcal{T}^k\delta(t)\mathbf{n}(0). \quad (14)$$

If we compute the iterates of $\mathcal{T}$ acting on $\mathbf{q}^{(0)}(t)$, we see that the successive terms $\mathcal{T}^k\mathbf{q}^{(0)}(t)$, with $\mathbf{q}^{(0)}(t) = \mathbf{n}^{(0)}\delta(t)$, account for the probability to arrive on a given node at time t, starting from the initial condition $\mathbf{n}^{(0)}$, in exactly k steps.

Remark 2. In general, the Neumann series does not offer a practical way for computing $(I-\mathcal{T})^{-1}$ since it involves an infinite number of terms. Because we make the assumption that the underlying graph $\mathcal{G}$ has no cycles, the series can be cut after d terms, where d is the diameter of the graph.

Based on (3) we can now compute $\dot{\mathbf{n}}(t)$ in terms of the transition density and of the initial conditions. Applying Leibniz's rule for differentiation under the integral sign, we obtain

$$\dot{n}_i(t) = q_i(t) - \int_0^t q_i(\tau)\sum_{j\in V_i} T_{ji}(t,\tau)d\tau = q_i(t) - \int_0^t q_i(\tau)T_{\bullet i}(t,\tau)d\tau. \quad (15)$$

The interpretation is that the rate of evolution of $n_i(t)$ is given by a sum of all arrivals minus the departures, with each departure resulting from a previous arrival at any point in time. Let us define a diagonal integral operator $\mathcal{D}$ acting on $\mathbf{q}$ by its ith component:

$$[\mathcal{D}\mathbf{q}(t)]_i = \int_0^t T_{\bullet i}(t,\tau)q_i(\tau)d\tau. \quad (16)$$

Equation (15) can now be written as

$$\dot{\mathbf{n}}(t) = (I - \mathcal{D})\mathbf{q}(t) = (I - \mathcal{D})\sum_{k=0}^{\infty} \mathcal{T}^k \mathbf{q}^{(0)}(t), \tag{17}$$

where we have used (13) to obtain the second equation.

C. Transition density on DAGs

The equation for $\mathbf{n}(t)$ remains abstract unless we can write T_{ji} explicitly in terms of the model parameters contained in Fig. 2. For the sake of simplicity and without lack of generality in the reasoning, we assume that all edges share the same up-time and down-time densities: $U_{ij}(t) =: U(t)$ and $D_{ij}(t) =: D(t)$, for all $i, j = 1, \ldots, N$.

Let p denote the probability that a given edge of $\mathcal{G}$ is active (up state) at a random time. Recall that we assume up-time and down-time durations with finite expectation. It results that

$$p = P\{\text{edge } i \to j \text{ is active}\} = \frac{\langle U \rangle}{\langle U \rangle + \langle D \rangle}, \tag{18}$$

where $\langle f \rangle = \int_{\mathbb{R}} t f(t) dt$ is the mathematical expectation of the random variable with PDF $f(t)$. We decompose the transition density in two terms: $T_{ji}(t, \tau) = (\mathbf{1}) + (\mathbf{2})$. The first term corresponds to the case that an edge is available to the jumper at the end of his waiting time:

$$(\mathbf{1}) = \psi_i(t - \tau) \sum_{k=1}^{|V_i|} \frac{1}{k} \binom{|V_i| - 1}{k - 1} p^k (1 - p)^{|V_i| - k}. \tag{19}$$

Edge $i \to j$ has to be available, and needs to be chosen amongst the $|V_i| - 1$ other edges which are also active at time t. A straightforward computation allows us to rewrite Eq. (19) as

$$(\mathbf{1}) = \psi_i(t - \tau) \frac{1}{|V_i|} [1 - (1 - p)^{|V_i|}]. \tag{20}$$

The quantity between square brackets is the probability that at least one edge is available. The factor $1/|V_i|$ appears because all outgoing edges are treated indifferently, and so the probability to be chosen is distributed uniformly amongst all edges including $i \to j$.

In the second case represented by Fig. 4, the jump occurs after the walker happened to be trapped. Let us observe that when the walker becomes trapped on node i, then for a given $j \in V_i$ the time w before $i \to j$ becomes available has the PDF

$$\mathscr{D}(t) = \frac{1}{\langle D \rangle} \int_t^{\infty} D(v) dv \tag{21}$$

as follows from the so-called bus paradox.

Edge $i \to j$ is selected by the trapped walker to perform the jump a time t if (i) the waiting time expires before t, (ii) at that moment all other edges are not active and will remain inactive at least until t, and (iii) edge $i \to j$ was also down but becomes active exactly at time t. It results that

$$(\mathbf{2}) = \int_{\tau}^{t} \psi_i(x - \tau) [(1 - p) P\{w > t - x\}]^{|V_i| - 1} \times (1 - p) \mathscr{D}(t - x) dx \tag{22}$$

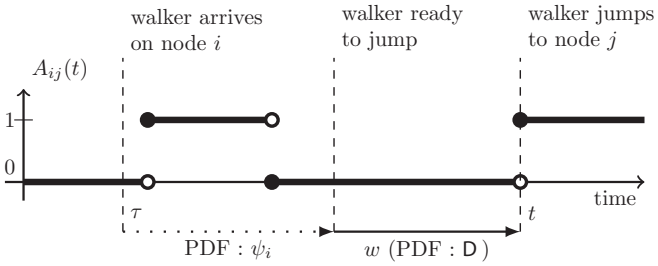

FIG. 4. Waiting time w of the trapped walker on node i, before edge $i \to j$ becomes active. The walker arrived at time τ on node i. After a waiting time determined by the density $\psi_i(t)$, a jump can be performed but none of the $|V_i|$ outgoing edges is active. The walker needs to wait a subsequent duration w before a link—here to node j—becomes available. So eventually the jump is performed at time t.

or in a slightly more compact way,

$$(\mathbf{2}) = (1 - p)^{|V_i|} \int_{\tau}^{t} \psi_i(x - \tau) \mathscr{D}(t - x) \times [P\{w > t - x\}]^{|V_i| - 1} dx, \tag{23}$$

where

$$P\{w > t - x\} = \int_{t-x}^{\infty} \mathscr{D}(s) ds. \tag{24}$$

In short, we have shown that

$$T_{ji}(t, \tau) = c_1 \psi_i(t - \tau) + c_2 \int_{\tau}^{t} \psi_i(x - \tau) \times \left[\int_{t-x}^{\infty} \mathscr{D}(s) ds \right]^{|V_i| - 1} \mathscr{D}(t - x) dx, \tag{25}$$

where c_1 and c_2 depend only on $\langle U \rangle$, $\langle D \rangle$, and $|V_i|$. For the sake of readability, we have dropped the index i due to the node dependence of c_1 and c_2. Observe that the distribution of U only matters through its mean, because only the mean value $\langle U \rangle$ influences the probability p. On the other hand, if the walker is ready to jump during a down time, then the jumps occur directly at the end of this down time, and so the full distribution of D does matter.

Remark 3. Having assumed an acyclic directed network allows us to consider all outgoing edges the same way. There is no possibility for the walker to backtrack to its previous step. The time when an edge becomes available to the walker does not depend on the arrival time of the walker on the node, and the density $\mathscr{D}$ of w can be applied for all outgoing edges. Indeed, if on the contrary the walker could jump across the cycle $i \to j \to i$, the probability for link $i \to j$ to still last can be large. This would induce a bias on the next jump, giving it more chance to end up again in j. It results that, as stated before, $T_{ji}(t, \tau)$ depends on the variables t and τ through their difference $t - \tau$.

Remark 4. Also observe that the transition density is the same for all $j \in V_i$, but the number of outgoing neighbors matters and appears in the transition density via the strength $|V_i|$ of node i in the underlying graph.

TABLE I. Selected particular cases. Here, δ means a dirac distribution in 0 and $\mathcal{E}(x)$ stands for exponential with rate x.

	$\psi_i(t)$	$U(t)$	$D(t)$
Case 1	δ	δ	$\mathcal{E}(\lambda)$
Case 2	$\mathcal{E}(\mu)$	δ	$\mathcal{E}(\lambda)$
Case 3	$\mathcal{E}(\mu)$	$\mathcal{E}(\eta)$	$\mathcal{E}(\lambda)$

D. Limit cases on DAGs

In this section we shortly discuss some particular cases listed in Table I.

1. Case 1

In this case the duration of each up time of a link is instantaneous. The down time is exponentially distributed with rate λ while the walker's waiting time is again instantaneous meaning the agent is always ready to jump. It is then straightforward to see that the waiting time of a trapped walker before a given edge activates has density

$$\mathscr{D}(x) = \frac{1}{1/\lambda}\int_x^\infty \lambda e^{-\lambda s} ds = \lambda e^{-\lambda x} = D(x), \tag{26}$$

which results from the memorylessness of the exponential distribution. Moreover, the probability for an edge to be up at a random time is $p = 0$, and it follows that (25) is computed as

$$\begin{aligned} T_{ji}(t,\tau) &= [P\{w > t-\tau\}]^{|V_i|-1}\mathscr{D}(t-\tau) \\ &= \left[\int_{t-\tau}^\infty \mathscr{D}(s)ds\right]^{|V_i|-1}\mathscr{D}(t-\tau) \\ &= \frac{1}{|V_i|}\lambda\,|V_i|\,\exp[-\lambda\,|V_i|\,(t-\tau)]. \end{aligned} \tag{27}$$

The first factor results from the choice of one of the edges (uniformly) in the underlying graph, while the second factor shows the distribution is again exponential, with rate $\lambda\,|V_i|$. This is the density of the minimum of $|V_i|$ exponential distributions with parameter λ. Recall that $T_{ji}(t,\tau)$ depends only on the difference $t-\tau$ and on parameters of $\mathcal{G}$. This shows that the dynamics amounts to a Poisson CTRW on a static graph. In this sense, we recover the result of [22].

Remark 5. If the down time is not exponentially distributed, it is still true that the transition density is written in terms of the density $\mathscr{D}_{(1),i}$ corresponding to the minimum of $|V_i|$ independent random variables with density $\mathscr{D}$:

$$T_{ji}(t,\tau) = \frac{1}{|V_i|}\mathscr{D}_{(1),i}(t-\tau). \tag{28}$$

It is a straightforward calculation to see that

$$\begin{aligned} \mathscr{D}_{(1),i}(t) &= -\frac{d}{dt}[P(w>t)]^{|V_i|} \\ &= |V_i|[1-F_w(t)]^{|V_i|-1}\mathscr{D}(t), \end{aligned} \tag{29}$$

where $F_w(t)$ is the distribution function of the variable w with density $\mathscr{D}$.

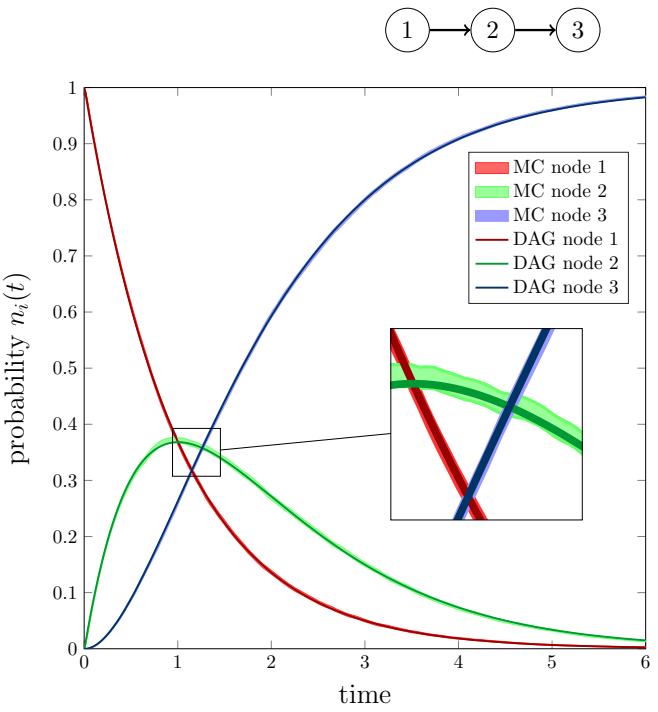

FIG. 5. Validation of the analytical model on a DAG in case 3 of Table I. All densities are exponential: $\psi \sim \mathcal{E}(\mu = 1)$, $U \sim \mathcal{E}(\eta = 1)$, $D \sim \mathcal{E}(\lambda = 1)$. The Monte Carlo simulation is the average of 10^5 independent trajectories of a single walker and yields the shaded areas representing a confidence interval of one standard deviation above and below the mean. The solid curves represent the probabilities $n_i(t)$ obtained from the analytical model. The inset magnifies the central part of the main figure, and shows clearly that the modeling falls in line with the numerical simulations. The graph is a directed chain with three nodes, as shown in the top right corner.

2. Cases 2 and 3

In these two cases, the computation of T_{ji} and Φ_i yield compact expressions (see Appendixes A and B). The exactness of the expressions result from the network being acyclic. An integration of the analytical model is compared against Monte Carlo simulation on Fig. 5 in case 3 where all distributions are exponential.

E. Equivalent node- and edge-centric models

In all possible cases (thus beyond exponential distributions), the model for DAGs can be cast into a nodes-only process on a static network, or into an edges-only process with instantaneous durations of edges availability, and a walker with no waiting time.

In the former case for instance, only a waiting-time density of the walker is retained, and it can be computed from the densities ψ, U, and D of the original model. For the sake of compactness, we assume all edges to follow the same densities. The all-in-one waiting-time PDF for the walker in node i with $|V_i| > 0$ is

$$\Psi_i(t) = (\psi_i * \widetilde{\mathcal{D}}_{(1),i})(t), \tag{30}$$

where $*$ denotes a convolution in the time variable and with

$$\widetilde{\mathcal{D}}_{(1),i}(t) = (1-p)^{|V_i|}\mathcal{D}_{(1),i}(t) + [1-(1-p)^{|V_i|}]\delta(t). \quad (31)$$

It results that

$$\Psi_i(t) = (1-p)^{|V_i|}(\psi_i * \mathcal{D}_{(1),i})(t) + [1-(1-p)^{|V_i|}]\psi_i(t). \quad (32)$$

The model reduction in the edge-centric case can be deduced from this formula. Let X_i be the random variable with density Ψ_i and let $Y_{i\bullet}$ be the random variable for the waiting time associated in the reduced model to an edge originating from node i with degree $|V_i| > 0$. Then X_i is the minimum of $|V_i|$ independent and identically distributed (i.i.d.) random variables such as $Y_{i\bullet}$ and we know

$$F_{X_i}(t) = 1 - (1 - F_{Y_{i\bullet}})^{|V_i|}, \quad (33)$$

yielding

$$F_{Y_{i\bullet}}(t) = 1 - [1 - F_{X_i}(t)]^{1/|V_i|}. \quad (34)$$

The PDF $\Delta_{i\bullet}$ of the waiting time on the edge can be obtained via

$$\Delta_{i\bullet}(t) = \frac{1}{|V_i|}[1 - F_{X_i}(t)]^{1/|V_i|}\Psi_i(t). \quad (35)$$

IV. CYCLES AND EMERGENCE OF MEMORY

The random walk under scrutiny in this work involves three processes, each with its own time scale and characterized by the densities ψ_i, U, and D. Section II and Fig. 2 in particular offered a qualitative evidence of three possible scenarios. In the first one, the durations of the down times are fast with respect to the typical walkers' waiting time, and node-centric modeling proves applicable. In the second one, the down times (respectively the up times) are relatively slow (respectively fast) as compared to the walker, and edge-centric modeling is effective. In the third scenario however, when none of the two previous assumptions holds true, the modeling needs not neglect any of the three processes. This claim is hereby sustained by Fig. 6 where the evolution of $\mathbf{n}_{\text{Monte Carlo}}(t)$ from 5×10^3 Monte Carlo simulations is compared with the predictions from the active node-centric and the passive edge-centric models, in the all-exponential case. In the former model, the dynamics of the edges is neglected: a static network is assumed and the master equation is

$$\dot{\mathbf{n}}_{\text{active}} = -\mathbf{n}_{\text{active}}(I - \text{diag}(|V_1|, \ldots, |V_N|)^{-1}G), \quad (36)$$

where G is the adjacency matrix of the underlying network $\mathcal{G}$ and the time is scaled by the rate μ of the walker. In the latter case, the walker has no own waiting time. The dynamics between the up times of the edges is accounted for, while the up times themselves are instantaneous. Therefore, the time is scaled according to the rate λ of the down times and

$$\dot{\mathbf{n}}_{\text{passive}} = -\mathbf{n}_{\text{passive}}(\text{diag}(|V_1|, \ldots, |V_N|) - G). \quad (37)$$

The norm of the error between the numerical simulation and the two models is then integrated over the duration T of the simulations,

$$E_{\text{model}}(T) = \int_0^T \|\mathbf{n}_{\text{model}}(s) - \mathbf{n}_{\text{Monte Carlo}}(s)\|_2 ds, \quad (38)$$

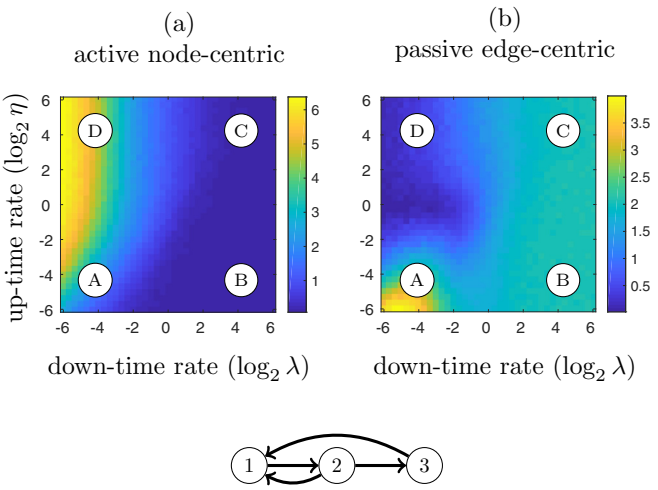

FIG. 6. Comparison of the classical active node-centric (a) and passive edge-centric (b) models with a Monte Carlo simulation involving 5×10^3 independent trajectories. The errors $E_{\text{active}}(T)$ and $E_{\text{passive}}(T)$ between the predictions of the models and the actual (Monte Carlo) probabilities $n_i(t)$ as given by Eq. (38) are plotted for various combinations of the rates of the exponential up-time and down-time densities η and λ. The walker's exponential density has rate $\mu = 1$ on all nodes. Each of the four regimes marked by the letters $A-D$ correspond to the four scenarios previously identified on Fig. 2. Section IV aims at providing the necessary modeling framework to cover the full domain of this plot, and to even go beyond the case considered here, allowing not clearly separated time scales. The graph appears at the bottom of the figure, and the duration of the simulations is $T = 10$.

where "model" stands for "active" or "passive." Note that in the three preceding equations, $\mathbf{n}_{\text{model}}$ is a row vector. The outcome is represented by Fig. 6 in the $(\log_2 \lambda, \log_2 \eta)$ plane, having chosen a rate $\mu = 1$ for ψ_i on the nodes.

The region where both errors are large demonstrates the need for the inclusive model developed in Sec. III, where the full interplay of the walker's and edges' behaviors are accounted for. The results derived thus far relied on an assumption of independence between events, i.e., links creation and destruction, encountered by the random walker. This assumption is clearly valid for DAGs but ceases to hold true when the underlying network has cycles. In that case, the walker may be influenced by the statistical information left at the previous passage, which may induce biases in the walker's trajectory [23,24]. The acyclic predictions are however expected to remain good approximations if the process on the nodes (ψ) is slow with respect to the edges dynamics, either in the case of long cycles or also locally if nodes have a high degree. In other cases, as illustrated in Fig. 7, one can observe significant deviations between the approximation and the numerical simulations of the process, even in situations when each of the three processes is a Poisson process. In such cases, we will observe the emergence of memory, or loss of the Markov property, in the trajectories of the walker.

In general, if cycles are present in the network, the state space is the full trajectory of the random walk, which makes the problem intractable analytically. We hereby propose a method estimating the corrections due to cycles of a given

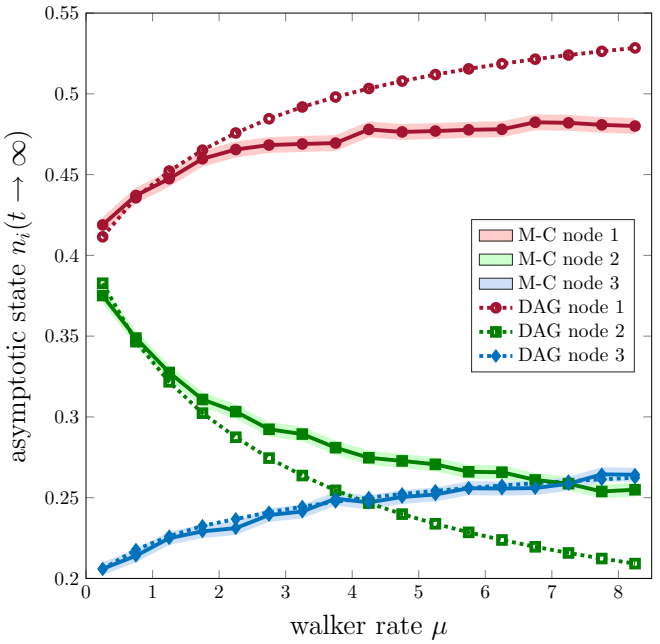

FIG. 7. The formulas for DAGs are no longer valid if there are cycles, as can be seen from this comparison with Monte Carlo simulations. In this figure, the stationary state $n_i(t \to \infty)$ in each node for varying values of the rate μ of the exponential density of the walker's waiting time $\psi(t)$ is plotted resulting from Monte Carlo simulation (solid lines with filled markers) and the analytical model on DAG's (dotted lines with empty markers). The width of the shading around the Monte Carlo curves corresponds to twice the standard deviation of the mean computed on 4×10^4 independent trajectories. The up and down time also follows exponential distributions, $U \sim \mathcal{E}(\eta = 1)$, $D \sim \mathcal{E}(\lambda = 1)$, and the initial condition of the walk is $\mathbf{n}(0) = (1, 0, 0)^T$. This example illustrates that when the time scale of the walker is faster, the memory effect becomes more pronounced and the error with respect to the Monte Carlo simulations increases. The graph is the one of Fig. 6.

length, and which generalizes the results in Sec. III. Although the proposed framework is general, we restrict the following discussion to contributions of cycles of length 2. This choice is motivated by the sake of simplicity and speeds up numerical simulations, as the incorporation of long cycles comes with increased computational cost. Also note that longer cycles are associated to weaker corrections, as more time between two passages tends to wash out footprints left by the walker.

A. Master equation with corrections for two-cycles

We need to enlarge the state space of the system in order to allow a correction for two-cycles. Let us accordingly first define $q_{imm'}(\tau, \nu)$ to be the arrival time density for the couple (τ, ν) on nodes $m' \to m \to i$. Observe that almost surely, $0 < \nu < \tau$. As depicted by Fig. 8, let $T_{j|imm'}(t|\tau, \nu)$ be the conditional transition density across edge $i \to j$ at time t, taking the two previous jumps into account: from m' to m at time ν and from m to i at time τ. It will become clear that by the limited amount of memory we take into account, this conditional density actually only depends on the durations $t - \nu$ and $\tau - \nu$. Let also $\Phi_{imm'}(t|\tau, \nu)$ be the probability to

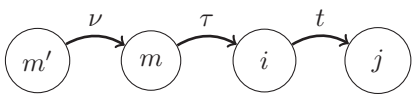

FIG. 8. Jump times and nodes in the definition of the transition density $T_{j|imm'}(t|\tau, \nu)$. The arrows are labeled by the jump time. Here, nodes m' and i and nodes m and j are not necessarily different nodes.

stay up to time t on node i, having arrived at time τ in the node, and having made the two previous jumps at times $\nu \leqslant \tau$ as represented by Fig. 9. We have

$$\Phi_{imm'}(t|\tau, \nu) = 1 - \sum_{j \in V_i} \int_\tau^t T_{j|imm'}(s|\tau, \nu)\, ds. \tag{39}$$

The normalization condition reads

$$\lim_{t \to \infty} \Phi_{imm'}(t|\tau, \nu) = 0, \quad \forall\, 0 \leqslant \nu \leqslant \tau, \tag{40}$$

and so

$$\sum_{j \in V_i} \int_\tau^\infty T_{j|imm'}(s|\tau, \nu)\, ds = 1, \tag{41}$$

for all $0 \leqslant \nu \leqslant \tau$ and $1 \leqslant i \leqslant N$. In the remainder of this section the computations assume the conditional transition density to be known. Its exact form will be determined in the next section.

Using the same steps as for acyclic graphs, let us first write the probability that the walker is on node i at time t as

$$n_i(t) = n_i^{(0)}(t) + n_i^{(1)}(t) + n_i^{(k \geqslant 2)}(t), \tag{42}$$

where the superscript refers to the number of jumps performed up to time t. The first two terms are not impacted by the memory effect, and can be computed based on the transition densities established under the no-cycle hypothesis:

$$n_i^{(0)}(t) = \int_0^t q_i^{(0)}(t)\Phi_i(t, \tau)d\tau = n_i(0)\Phi_i(t, 0), \tag{43}$$

and

$$\begin{aligned} n_i^{(1)}(t) &= \int_0^t q_i^{(1)}(\tau)\Phi_i(t, \tau)d\tau \\ &= \sum_{m \in V_i'} n_m(0) \int_0^t T_{im}(\tau, 0)\Phi_i(t, \tau)d\tau. \end{aligned} \tag{44}$$

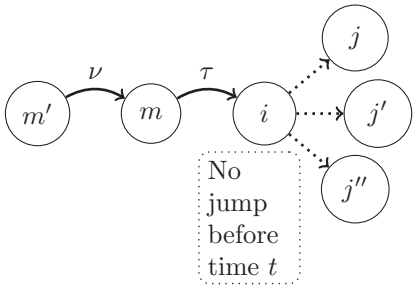

FIG. 9. Jump times and nodes in the definition of the probability $\Phi_{imm'}(t|\tau, \nu)$. The arrows are labeled by the jump time. Nodes m' and i could be the same node.

It remains to compute $n_i^{(k\geqslant 2)}(t) = \sum_{k\geqslant 2} n_i^{(k)}(t)$. Note that in $n_i^{(k)}(t)$ we also need the transition density of the $(k+1)$th jump which determines the probability to stay put on node i up to time t after k jumps. For all $k \geqslant 2$ one can write

$$n_i^{(k)}(t) = \sum_{m'\to m\to i}\sum \iint_{0\leqslant\nu\leqslant\tau} q_{imm'}^{(k,k-1)}(\tau,\nu) \times \Phi_{imm'}(t|\tau,\nu)\,d\nu d\tau, \tag{45}$$

where again the superscript in $q_{imm'}^{(k,k-1)}$ gives the number of jumps. In order to determine $n_i^{(k\geqslant 2)}(t)$ we will need

$$q_{imm'}(\tau,\nu) = \sum_{k\geqslant 2} q_{imm'}^{(k,k-1)}(\tau,\nu). \tag{46}$$

Once we have computed this quantity, then the third term in (42), $n_i(t) = n_i^{(0)}(t) + n_i^{(1)}(t) + n_i^{(k\geqslant 2)}(t)$, will indeed follow as

$$n_i^{(k\geqslant 2)}(t) = \sum_{m'\to m\to i}\sum \iint_{0\leqslant\nu\leqslant\tau} q_{imm'}(\tau,\nu) \times \Phi_{imm'}(t|\tau,\nu)\,d\nu d\tau, \tag{47}$$

and we have obtained the probability $n_i(t)$ in function of the initial condition $\mathbf{n}(0)$.

Let us therefore determine the arrival-times density in a given number of jumps, $q_{imm'}^{(k,k-1)}(\cdot,\cdot)$. Let us write Eq. (46) by splitting the sum as

$$q_{imm'}(\tau,\nu) = \sum_{k=2}^{\infty} q_{imm'}^{(k+1,k)}(\tau,\nu) + q_{imm'}^{(2,1)}(\tau,\nu). \tag{48}$$

In this expression, for all $k \geqslant 2$,

$$q_{imm'}^{(k+1,k)}(\tau,\nu) = \sum_{m''\in V_{m'}'} \int_0^\nu T_{i|mm'm''}(\tau|\nu,\nu') \times q_{mm'm''}^{(k,k-1)}(\nu,\nu')\,d\nu' \tag{49}$$

and using again (46), Eq. (48) becomes

$$q_{imm'}(\tau,\nu) = \sum_{m''\in V_{m'}'} \int_0^\nu T_{i|mm'm''}(\tau|\nu,\nu') \times q_{mm'm''}(\nu,\nu')\,d\nu' + q_{imm'}^{(2,1)}(\tau,\nu). \tag{50}$$

The extended initial condition of arrival times for the first two jumps is given by

$$q_{imm'}^{(2,1)}(\tau,\nu) = \widetilde{T}_{im}(\tau-\nu)\int_0^\nu \widetilde{T}_{mm'}(\nu-\nu')q_{m'}^{(0)}(\nu')d\nu' = \widetilde{T}_{im}(\tau-\nu)\widetilde{T}_{mm'}(\nu)n_{m'}(0), \tag{51}$$

where $\widetilde{T}_{ji}(t) := T_{ji}(t,0)$ is the transition density for the acyclic case.

Equation (50) is a Volterra linear integral equation of the second kind, with kernel given by the conditional transition density that is determined hereafter. We have a vector of unknown functions $\mathbf{Q}$, where each component function $q_{imm'}(\cdot,\cdot) : [0,\infty)^2 \to [0,\infty)$ corresponds to a path of length 2 in the underlying graph $\mathcal{G}$. As will appear clearly in the sequel, this equation cannot be cast under the form of a convolution, because as we will see $T_{i|mm'm''}(\tau|\nu,\nu') = T_{i|mm'm''}(\tau-\nu'|\nu-\nu',0)$. Consequently, the Laplace-transform-based method cannot be applied.

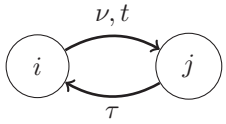

FIG. 10. Jump times and edges through which the jumps occur in the transition density $T_{j|iji}(t|\tau,\nu)$. The arrows are labeled by the jump time. Note that node i can possibly have other out neighbors than j. The corresponding edges would then impact the transition density through edge $i \to j$.

B. Transition density with correction for two-cycles

We want to compute $T_{j|imm'}(t|\tau,\nu)$. The trajectory before the jump at time ν is not taken into account and so only durations starting from time ν matter:

$$T_{j|imm'}(t|\tau,\nu) = T_{j|imm'}(t-\nu|\tau-\nu,0). \tag{52}$$

Therefore, we need to determine $\widetilde{T}_{j|imm'}(x|y) := T_{j|imm'}(x|y,0)$, $0 \leqslant y \leqslant x$. There are three cases, depending on whether $(m' \to m \to i)$ is a two-cycle or not.

(i) In the first case, $m' \neq i$, and there is no memory effect due to two-cycles. The density reads as before

$$\widetilde{T}_{j|imm'}(x|y) = \widetilde{T}_{ji}(x-y), \tag{53}$$

where the right-hand side is the one from the modeling for DAGs.

(ii) In the second case, $(m',m) = (i,j)$ and we have the situation depicted by Fig. 10. The density cannot be written in terms of the one obtained for acyclic graphs.

(iii) In the third case, $m' = i$ but $m \neq j$, as shown in Fig. 11, and again, we do not have a reduction like in Eq. (53).

By definition, $\widetilde{T}_{j|imm'}(x|y) = T_{j|imm'}(x|y,0)$ with $x = t-\nu$ and $y = \tau-\nu$. In the following, the letters t,τ,ν will indicate absolute times, whereas x and y are durations. We will keep both in order to avoid having to assume a jump a time 0. As before, in the second and third cases, we will write

$$\widetilde{T}_{j|imm'}(x|y) = (\mathbf{1}) + (\mathbf{2}), \tag{54}$$

where the first term corresponds to a jump at the end of the waiting time on the node, whereas the second term is for the jump of a trapped walker. The computation of both terms requires us first to determine the probability for an edge to

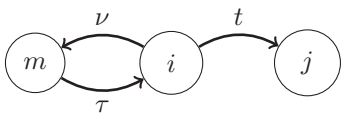

FIG. 11. Jump times and edges corresponding to the jumps in the transition density $T_{j|imi}(t|\tau,\nu)$. The arrows are labeled by the jump time. Here, m and j are assumed to be different nodes. Not all out neighbors of node i are represented, although they would influence the transition density.

be (un)available some time after having (not) jumped across it.

1. Corrections on $p = \langle U\rangle/(\langle U\rangle + \langle D\rangle)$

When the walker returns to a node after completion of a two-cycle, the next destination node depends on the choice previously made from the same location. First, the outgoing edge that was selected at the beginning of the cycle, say $i \to j$, has an increased probability [with respect to $p = \langle U\rangle/(\langle U\rangle + \langle D\rangle)$] to still be available. The smaller the time $y = \tau - \nu$ to go through the cycle and the subsequent walker's waiting time, the more pronounced this effect. Second, the converse is also true for any edge, say $i \to j'$, that wasn't selected. Not having been chosen in the past indicates a higher probability to have been and still be down some short time later. In the main body, we present the derivation for the first effect,

$$p_i^*(s,\nu) = P\{i \to j \text{ is up at } s \,|\, \text{jumped across it at } \nu\}, \quad (55)$$

whereas Appendix C contains the computations for the second effect quantified by

$$p_i^\dagger(s,\nu) = P\{i \to j' \text{ is up at } s \,|\, \text{jumped across } i \to j \text{ at } \nu\} \quad (56)$$

for some $s \geqslant \nu$ and $j' \neq j$. Let us focus on the first effect, measured by the difference between $p^*(s,\nu)$ and p. Observe that this function only depends on the difference $s - \nu$. Let us define $\tilde{q}_i$, the probability that the jump $i \to j$ at time ν was done at the beginning of an up time, that is to say, the walker was frustrated at the time of the jump. Observe that we do not know the effective waiting time on the node before the jump (a longer waiting time would have made a jump after a frustration period more plausible). Hence, assuming no memory beyond the last two jumps we have

$$\tilde{q}_i = (1-p)^{|V_i|}. \quad (57)$$

Let us also define

$$\widetilde{U}_i(x) = \tilde{q}_i U(x) + (1-\tilde{q}_i)\mathscr{U}(x), \quad x \geqslant 0, \quad (58)$$

the density of the remaining up time of edge $i \to j$ after the jump at time ν was performed, where $\mathscr{U}$ is computed similarly to (21): $\mathscr{U}(x) = 1/\langle U\rangle \times \int_x^\infty U(x')dx'$.

Remark 6. The value of $\tilde{q}_i$ is irrelevant in Eq. (58) if U is an exponential density, because then $U = \mathscr{U}$. In that case, $\widetilde{U}_i$ does not depend on the strength of node i in $\mathcal{G}$ and we will drop the node-related index.

As illustrated by Fig. 12, we can write

$$\begin{aligned} p_i^*(s,\nu) = &\int_{s-\nu}^\infty \widetilde{U}_i(r)dr + \int_0^{s-\nu} (\widetilde{U}_i * D)(r) \\ &\times \int_{s-(\nu+r)}^\infty U(t)\,dt\,dr + \int_0^{s-\nu} (\widetilde{U}_i * D * U * D)(r) \\ &\times \int_{s-(\nu+r)}^\infty U(t)\,dt\,dr + \cdots . \end{aligned} \quad (59)$$

Introducing the notation for repeated convolutions

$$f^{*k_1} * g^{*k_2} = \underbrace{f * \cdots * f}_{k_1 \text{ factors}} * \underbrace{g * \ldots * g}_{k_2 \text{ factors}}, \quad k_1, k_2 \in \mathbb{N}, \quad (60)$$

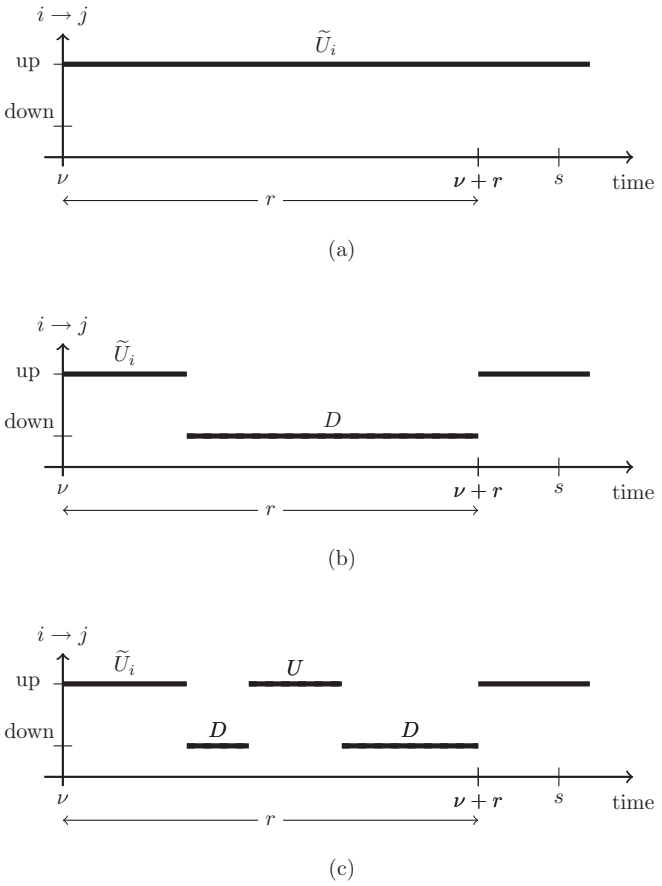

FIG. 12. Parameters involved in the computation of $p_i^*(s,\nu)$. Panels (a)–(c) represent respectively the first, second, and third terms in Eq. (61). The three corresponding scenarios are the following: either edge $i \to j$ remains up since time ν and up to time s, or it switches states twice before s, or it does so exactly four times on the interval (ν, s).

Eq. (59) has the compact form

$$\begin{aligned} p_i^*(s,\nu) = &\int_{s-\nu}^\infty \widetilde{U}_i(r)dr + \sum_{k=0}^\infty \int_0^{s-\nu} (\widetilde{U}_i * D^{*(k+1)} * U^{*k})(r) \\ &\times \int_{s-(\nu+r)}^\infty U(t)\,dt\,dr. \end{aligned} \quad (61)$$

Remark 7. In contrast with $p = \frac{\langle U\rangle}{\langle U\rangle+\langle D\rangle}$, the expression for p_i^* depends on the whole distribution of U, and not only on its mean. Also note that it only depends on the difference $s - \nu$, which is the time since the previous jump. See Fig. 14 for a numerical illustration in the all-exponential case.

2. Second case: $T_{j|iji}(t|\tau,\nu)$

Having computed the necessary corrections on p, we are now in position to further develop Eq. (54). The first term—the walker is not trapped when he jumps—reads

$$\begin{aligned} (\mathbf{1})_{(j|iji)} = \psi_i(t-\tau) \sum_{k=1}^{|V_i|} \frac{1}{k} p_i^*(t,\nu) \binom{|V_i|-1}{k-1} \\ \times (p_i^\dagger(t,\nu))^{k-1} (1 - p_i^\dagger(t,\nu))^{|V_i|-k} \end{aligned}$$

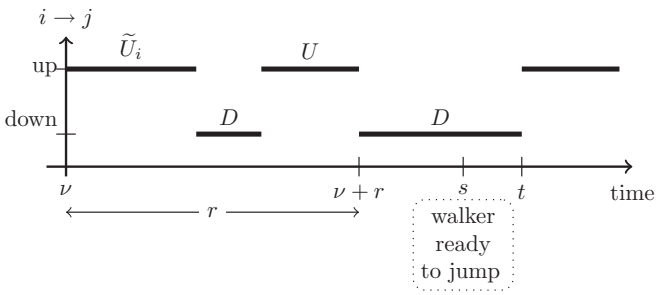

FIG. 13. Parameters involved in the second term of $T_{jiji}(t|\tau, \nu)$ given by Eq. (63). The figure corresponds to the term with $k = 1$, that is to say the first up time is followed by $k = 1$ down-up cycle.

$$= \frac{p^*(t,\nu)}{p_i^\dagger(t,\nu)} \psi_i(t-\tau) \left[\frac{1-(1-p_i^\dagger(t,\nu))^{|V_i|}}{|V_i|} \right]. \tag{62}$$

We notice that this expression is the same as for the acyclic graphs, up to a correction factor $p_i^*(t,\nu)/p_i^\dagger(t,\nu)$, and after having replaced p by $p_i^\dagger(t,\nu)$.

Using the same approach as for p_i^*, we obtain the second term of $T_{j|iji}(t|\tau,\nu)$ corresponding to a walker who was trapped before making the jump:

$$\begin{aligned}(\mathbf{2})_{(j|iji)} = \int_\tau^t \psi_i(s-\tau) \Bigg[\sum_{k=0}^{\infty} \int_0^{s-\nu} (\widetilde{U}_i * D^{*k} * U^{*k})(r) \\ \times D(t-\nu-r)\, dr \Bigg] \\ \times [(1-p_i^\dagger(s,\nu))P\{w > t-s\}]^{|V_i|-1}\, ds. \end{aligned} \tag{63}$$

The parameters are illustrated by Fig. 13. Relying on the previous computation of $p_i^*(s,\nu)$, expression (63) simplifies to the following one:

$$\begin{aligned}(\mathbf{2})_{(j|iji)} = \int_\tau^t \psi_i(s-\tau)(1-p_i^*(s,\nu))\mathscr{D}(t-s) \\ \times [(1-p_i^\dagger(s,\nu))P\{w > t-s\}]^{|V_i|-1}\, ds. \end{aligned} \tag{64}$$

In this alternative form, $(1-p_i^*(s,\nu))\mathscr{D}(t-s)$ refers to the probability that edge $i \to j$ is down at time s, and will remain so exactly until time t when it becomes available to the jumper again.

3. Third case: $T_{j|imi}(t|\tau,\nu)$ with $m \neq j$

The first term of the transition density in the case of Fig. 11 is given by

$$\begin{aligned}(\mathbf{1})_{(j|imi)} \\ = \psi_i(t-\tau)[p_i^*(t,\nu) \times P\{\text{choose } j \mid (i \to m) \text{ is up}\} \\ + (1-p_i^*(t,\nu)) \times P\{\text{choose } j \mid (i \to m) \text{ is down}\}], \end{aligned} \tag{65}$$

where the two still undetermined probabilities are for events at time t. We can write

$$\begin{aligned} &P\{\text{choose } j \mid (i \to m) \text{ is up}\} \\ &= p_i^\dagger(t,\nu) \sum_{k=0}^{|V_i|-2} \binom{|V_i|-2}{k} \\ &\quad \times \frac{1}{k+2} (p_i^\dagger(t,\nu))^k (1-p_i^\dagger(t,\nu))^{|V_i|-k-2} \\ &= \frac{|V_i| p_i^\dagger(t,\nu) + (1-p_i^\dagger(t,\nu))^{|V_i|-1}}{|V_i|(|V_i|-1)p_i^\dagger(t,\nu)} \end{aligned} \tag{66}$$

and

$$\begin{aligned} &P\{\text{choose } j \mid (i \to m) \text{ is down}\} \\ &= p_i^\dagger(t,\nu) \sum_{k=0}^{|V_i|-2} \binom{|V_i|-2}{k} \\ &\quad \times \frac{1}{k+1} (p_i^\dagger(t,\nu))^k (1-p_i^\dagger(t,\nu))^{|V_i|-k-2} \\ &= \frac{1-(1-p_i^\dagger(t,\nu))^{|V_i|-1}}{|V_i|-1}, \end{aligned} \tag{67}$$

where the final forms (66) and (67) were obtained as in Appendix C using identity (C8).

The second term can be shown to have the same expression as in Eq. (64).

C. All-exponential case of Table I

We turn to the case where the three densities are exponential: ψ has rate μ, U has rate η, and D has rate λ. Wherever possible, we drop the index of the node dependence, such that for instance p_j^* becomes p^*. Let us recall that in this case, $\mathscr{U} = U$ and $\widetilde{U} = U$.

The expression of p^* given in Eq. (61) and the second term of the transition density given in Eq. (63) both require us to compute the density $U^{*k} * D^{*k}$, which corresponds to the sum of the random variables $X_U^{(k)} + X_D^{(k)}$ where $X_U^{(k)}$ (respectively $X_D^{(k)}$) is the sum of k exponential random variables with parameter η (respectively λ). It is well known that $X_U^{(k)} \sim \text{Erlang}(k,\eta)$, and $X_D^{(k)} \sim \text{Erlang}(k,\lambda)$. Using [37] for the convolution of Erlang densities, we find that the density of $X_U^{(k)} + X_D^{(k)}$ is given by

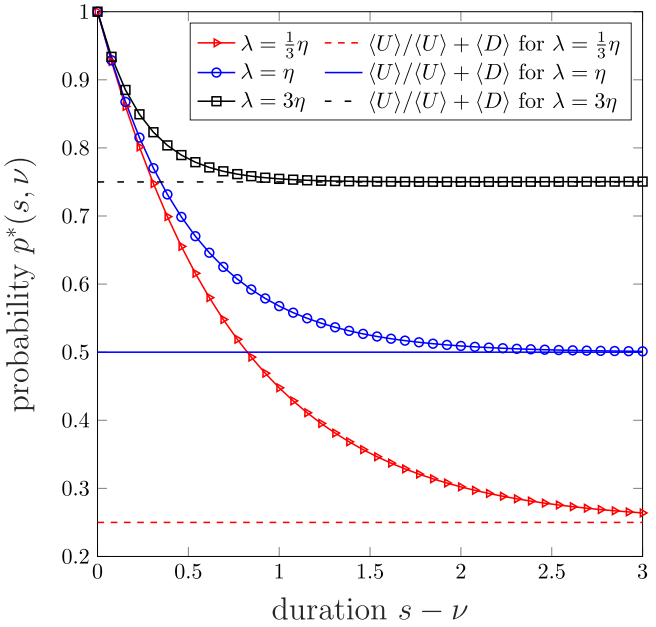

FIG. 14. Evolution of $p^*(s,\nu)$, i.e., the probability for an edge to be in the up state at time s knowing it was available at time ν, in the all-exponential case for various ratios of η/λ. The black series with square markers and the red one with triangle markers come from Eq. (69), whereas the blue series in the middle with circle markers corresponds to (70). In all three cases, the horizontal solid or dashed lines indicate the corresponding values of $p=\langle U\rangle/(\langle U\rangle+\langle D\rangle)$ that assumes no prior information.

$$f_{X_U^{(k)}+X_D^{(k)}}(t)=\frac{(\eta\lambda)^k}{(\lambda-\eta)^{2k}}\sum_{j=1}^{k}\left[\frac{(-1)^{k-j}}{(j-1)!}\binom{2k-j-1}{k-j}\right.$$
$$\left.\times(\lambda-\eta)^j\{e^{-\eta t}+(-1)^j e^{-\lambda t}\}\right]t^{j-1}\mathbb{1}_{\mathbb{R}^+}(t). \tag{68}$$

It follows that (61) becomes

$$p^*(s,\nu)=\int_{s-\nu}^{\infty}U(r)dr+\sum_{k=0}^{\infty}\int_0^{s-\nu}f_{X_U^{(k+1)}+X_D^{(k+1)}}(r)$$
$$\times\int_{s-(\nu+r)}^{\infty}U(t)\,dt\,dr. \tag{69}$$

Note again that index i is now needless. The above series can be truncated to allow for a practical computation. In the case that U and D share the same rate parameter λ, this expression further simplifies. A direct computation yields

$$p^*(s,\nu)=e^{-\lambda(s-\nu)}\cosh[\lambda(s-\nu)]=\tfrac{1}{2}(1+e^{-2\lambda(s-\nu)}). \tag{70}$$

The second term being positive is the increase with respect to $p=\frac{1}{2}$, and it is smaller for a higher rate λ and for larger $s-\nu$. This is because more up or down cycles will decrease the memory effect on the state of the edge. A numerical illustration of (69) and (70) is provided by Fig. 14.

On Fig. 15 the correctness of the first correction by p^* on p is assessed through comparison with a Monte Carlo simulation. In order to evaluate it independently from the

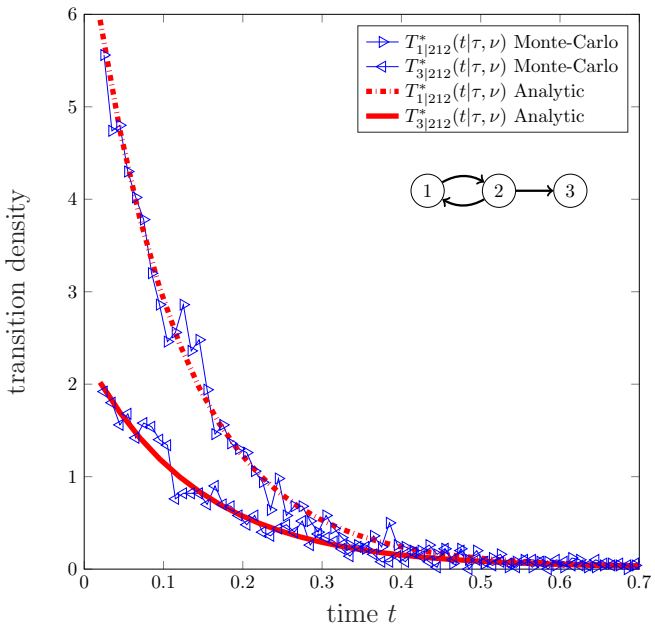

FIG. 15. Validation of the analytical formula for the memory effect related to $p^*(\cdot,\cdot)$ in the conditional transition density. The simultaneous effect of $p_i^\dagger(\cdot,\cdot)$ was annihilated by replacing it by p in the formulas of the density (red curves), which is therefore written with the superscript $*$ in the legend. The Monte Carlo simulation of 5000 independent trajectories (blue series with triangle markers) was designed so as to allow a memory effect solely on edge $2\to1$ of the graph appearing as an inset, thereby neglecting the effect corresponding to $p_i^\dagger$. The rate of the walker is $\mu=8$, the edges are characterized by the rates $\lambda=1=\eta$ and $\tau=0.02=2\nu$.

concurrent correction due to $p_i^\dagger$, we have set $p_i^\dagger(\cdot,\cdot)=p$ in the formulas of the conditional transition density, which is then written as $T^*_{j|imm'}(t|\tau,\nu)$ to highlight the change.

Let us consider the second correction on $p=\langle U\rangle/(\langle U\rangle+\langle D\rangle)$, which is quantified by $p_i^\dagger$. Assuming again the same rate for U and D, it follows directly from Eqs. (C13) and (C3) that

$$p_i^\dagger(s,\nu)=\tfrac{1}{2}-\tfrac{1}{4}e^{-2\lambda(s-\nu)} \tag{71}$$

when we set $|V_i|=2$, a choice that maximizes the importance of this effect. The second term represents the difference with respect to $p=\frac{1}{2}=2\tilde{q}_i$, and is such that $p_i^\dagger(s,\nu)\to\tilde{q}_i$ if $s-\nu\to0^+$ and $p_i^\dagger(s,\nu)\to p$ if $s-\nu\to+\infty$.

Combining the effects of p^* and $p_i^\dagger$ results in Fig. 16 where it appears clearly that a shorter time to go around the cycle $2\to1\to2$ induces a stronger bias in favor of another jump along $2\to1$ instead of $2\to3$.

A validation of the comprehensive analytical framework through a simple numerical example is the purpose of Fig. 17.

V. NUMERICAL METHODS

We solved the Volterra vector integral equations (9) and (50) by applying a trapezoidal scheme for discretization of the integrals, by a method described in Ref. [36]. The initial condition $\mathbf{q}^{(0)}(t)=\mathbf{n}(0)\delta(t)$ arising in these equations was approximated using a half-Gaussian-like positive function

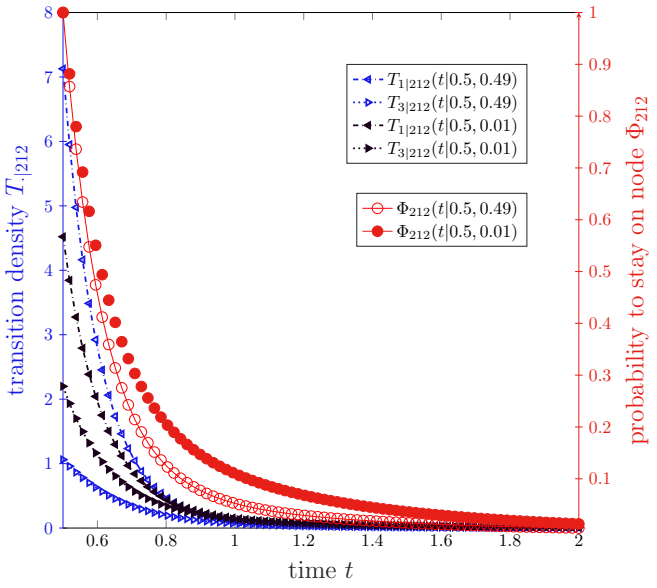

FIG. 16. Stronger (empty blue triangle markers) vs weaker (filled black triangle markers) memory effect depending on the time to go through a cycle. On the left vertical axis, one sees that the differentiation between the jump densities towards nodes 1 and 3, respectively, is more pronounced when the duration $\tau - \nu$ is smaller, and decreases with t. The resulting probabilities to stay put on node 2 are plotted in red on the right vertical axis. The empty circle markers correspond to a strong memory effect, and indicate a lower probability to remain for a long time on the node before a jump, when compared to the series with filled red circle markers (weaker memory). The graph is the one of Fig. 15. The rates are $\mu = 8$, $\eta = 1 = \lambda$, and $\tau = 0.5$, $\nu = 0.49$ for the strong effect, whereas $\tau = 0.5$, $\nu = 0.01$ in the other case.

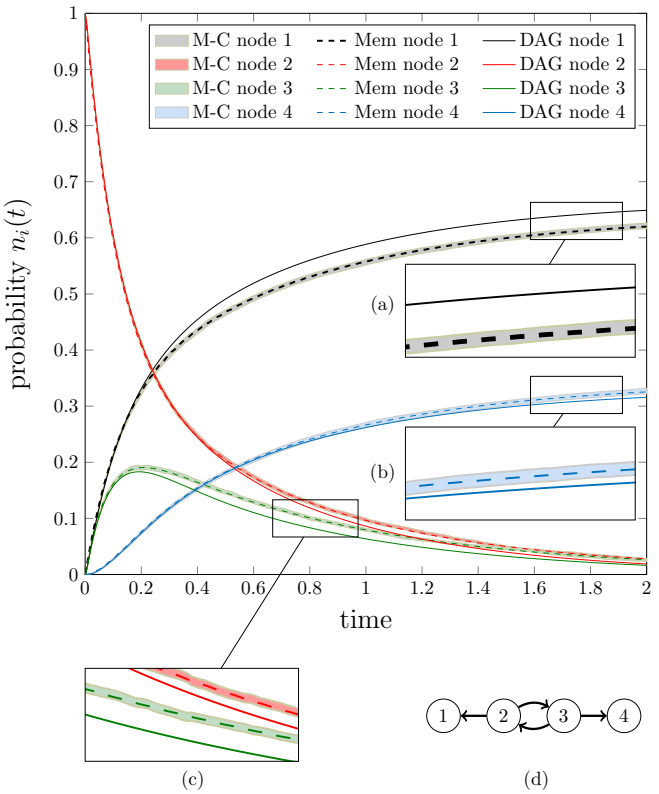

FIG. 17. Numerical validation of the analytical framework (dashed lines) accounting for the last-two-cycle memory effect. The Monte Carlo simulation (shading) results from the average of 4×10^4 independent trajectories of a single walker. The shaded areas determine an interval centered around the mean, of width equal to twice the standard deviation. In this simulation, the walker always starts in node 2 of the graph in panel (d). Due to the cycles effect, the increase of $n_i(t)$ for node 1 [inset (a)] is much slower when compared with the curve resulting from the transition densities valid for acyclic graphs (solid lines). Indeed, the memory effect comes into play only after (and if) the walker has completed the sequence $2 \to 3 \to 2$. This effect then acts in favor of node 4, for which the difference between the actual probability and the DAG approximation is less dramatic [inset (b)]. Also observe that the memory effect tends to bring the curves corresponding to the two nodes belonging to the cycle closer together [nodes 2 and 3, inset (c)]. By the same mechanism, the convergence of $n_2(t)$ and $n_3(t)$ to 0 is notably slower. The dashed series resulting from the analytical modeling with corrections are virtually indistinguishable from the Monte Carlo ones, which shows the effectiveness of the developed framework. The rates are $\mu = 8$, $\eta = 1 = \lambda$.

$\delta_\epsilon(t)$ parametrized by a small parameter ϵ, such that

$$\mathbf{q}^{(0)}(t) \approx \mathbf{n}(0)\delta_\epsilon(t), \qquad \int_0^\infty \delta_\epsilon(t)dt = 1. \tag{72}$$

The numerical method uses Monte Carlo simulation to determine the probabilities $\mathbf{n}(t)$ by averaging over a large set of realizations. Each trajectory of the walker corresponds to a new realization of the walker's waiting times and of the up and down time of the edges. The time interval $[0, T)$ of the simulation is discretized according to some partition $0 = t_0 < t_1 < \cdots < t_m = T$. The probability for the walker to be in some node over some time window $[t_k, t_{k+1}]$ is approximated by the mean over all simulations, of the fraction of time spent by the walker on that particular node. This is the same method as in Ref. [22].

VI. CONCLUSION

A very common assumption in the study of dynamical processes on networks is to take only the direction of the edges and their weights into account. Accordingly, one often assumes that temporal events on the edges occur as a Poisson process. An important contribution of the field of temporal networks is to question this assumption and to propose more complex temporal models, including renewal processes with arbitrary event-time distributions. Yet, in a majority of works, one considers, implicitly or explicitly, instantaneous interactions. The main purpose of this work was to incorporate edge duration in stochastic models of temporal networks, and to estimate its impact on random walk processes. We have derived analytical expressions for various properties of the process. As we have shown, those are exact on DAGs, and we have presented corrections due to the presence of cycles on the underlying network.

This work is mostly theoretical but it has plenty of potential applications in real-life systems. Take contact networks and their impact on epidemic or information spreading as a canon-

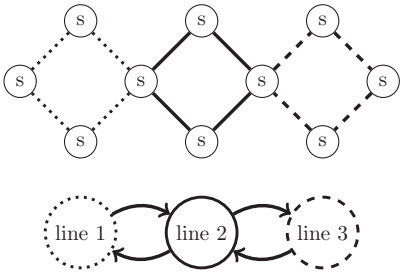

FIG. 18. A disruption-tolerant network based on mobile wireless sensors. The top schematic represents three independent bus lines, where two bus stops are shared by two different lines. The underlying network of allowed connections is given in the bottom graph.

ical example. For instance, recent research on empirical face-to-face network data collected via Bluetooth was performed by the authors of [30]. They looked into the predictability of the interactions between a large group of individuals taking part in the study. It is representative that their work would mostly rely on data, and doesn't go as far as spreading processes, where our modeling would come in handy. Indeed, in such context the underlying network can prove acyclic, at least at short time scales where few contacts are actually active, thereby simplifying the use of our formalism. But more importantly, the durations of availability time spans of the edges are inevitably finite and, as results from [38] and a wealth of publications relying on data collected by the SocioPatterns initiative [39,40], they feature a long-tailed distribution. This heterogeneity prohibits a well-defined time scale for the interactions, but can be captured by the proposed framework. In engineering, practical applications include peer-to-peer and proximity networks of mobile sensors with wireless connections (cast under the framework of DTN: disruption or tolerant networks). A good example would be the diffusion of buses in a city that can communicate only when they halt at the same bus stop [34] (see Fig. 18). Given the central role of random walks in the design of algorithms on networks, our results also open the way to generalize standard tools such as PageRank for centrality measures and Markov stability for community detection [12].

Yet, in our view, the key message of this paper is its emphasis on the importance of three time scales to characterize diffusion on temporal networks, one for diffusion and two for the edge dynamics. Future research directions include a more thorough investigation on when certain time scales can be neglected over other ones, hence leading to simplified mathematical models, and models including a fourth time scale, associated to the possible nonstationarity of the network evolution, for instance due to circadian rhythms.

APPENDIX A: TRANSITION DENSITY FOR DAGS IN CASE 2 OF TABLE I

When each up time of a link is instantaneous, $\langle U\rangle = 0$, $p = 0$ and the first term of $T_{ji}(t,\tau)$ vanishes. The second term yields

$$T_{ji}(t,\tau) = \mu\lambda e^{\mu\tau-\lambda|V_i|t}\int_\tau^t e^{(-\mu+\lambda|V_i|)x}dx. \tag{A1}$$

If $\mu = \lambda|V_i|$, the integral equals $t-\tau$ and $T_{ji}(t,\tau) = \lambda\mu(t-\tau)e^{-\mu(t-\tau)}$. Otherwise, a direct calculation yields

$$T_{ji}(t,\tau) = \frac{\lambda\mu}{\lambda|V_i|-\mu}(e^{-\mu(t-\tau)} - e^{-\lambda|V_i|(t-\tau)}). \tag{A2}$$

Observe that taking the limit $\mu\to\infty$ in the above expression yields

$$T_{ji}(t,\tau) = \frac{1}{|V_i|}\lambda|V_i|e^{-\lambda|V_i|(t-\tau)}, \tag{A3}$$

where the second factor is the density of the minimum of $|V_i|$ independent exponential densities with rate λ. We have recovered case 1. Starting from (A2) we have

$$\Phi_i(t,\tau) = \frac{1}{\lambda|V_i|-\mu}(\lambda|V_i|e^{-\mu(t-\tau)} - \mu e^{-\lambda|V_i|(t-\tau)}). \tag{A4}$$

The case that $\mu = \lambda|V_i|$ is straightforward.

APPENDIX B: TRANSITION DENSITY FOR DAGS IN CASE 3 OF TABLE I

When the up times of the links follow an exponential density $\mathcal{E}(\eta)$, we have $p = \frac{\lambda}{\lambda+\eta}$ and the first term of $T_{ji}(t,\tau) = (\mathbf{1}) + (\mathbf{2})$ reads

$$(\mathbf{1}) = \mu e^{-\mu(t-\tau)}\frac{1}{|V_i|}[1-(1-p)^{|V_i|}], \tag{B1}$$

whereas the second term $(\mathbf{2})$ in the more general case that $\mu \neq \lambda|V_i|$ is given by (A2) multiplied by $(1-p)^{|V_i|}$. Following a direct calculation, the probability to stay on node i for a time of at least $t-\tau$ now reads

$$\begin{aligned}\Phi_i(t,\tau) = 1-(1-p)^{|V_i|}\Bigg(1 - \frac{1}{\lambda|V_i|-\mu}\\ \times(\lambda|V_i|e^{-\mu(t-\tau)} - \mu e^{-\lambda|V_i|(t-\tau)})\Bigg)\\ -[1-(1-p)^{|V_i|}](1-e^{-\mu(t-\tau)}).\end{aligned} \tag{B2}$$

APPENDIX C: COMPUTATION OF $p_i^\dagger(s,\nu)$

We consider a two-cycle $i\to j\to i$ of the underlying graph $\mathcal{G}$ where node i has at least one neighbor j' other than j. For the sake of compactness, we compute $p^\dagger(s,\nu)$—the probability that edge $i\to j'$ is down at time s knowing it wasn't selected by the walker at time ν in the past—under the assumption that the durations $U(t)$ and $D(t)$ follow the same distribution. The reasoning readily applies without this assumption.

Let E_s and E_ν denote respectively the events that $i\to j$ is up at time s and at time ν. Let E'_s and E'_ν be the corresponding events for edge $i\to j'$ and let also F_ν be the event that the walker jumped through $i\to j$ at time ν. We

write $\bar{A}$ the complement of event A, such that $\mathrm{P}\{A \cup \bar{A}\} = 1$ and $\mathrm{P}\{A \cap \bar{A}\} = 0$. Using the law of total probabilities for conditional probabilities we have

$$\begin{aligned} p_i^\dagger(s,\nu) &= P\{E_s'|F_\nu\} \\ &= P\{E_s' \cap E_\nu'|F_\nu\} + P\{E_s' \cap \overline{E_\nu'}|F_\nu\} \\ &= P\{E_s'|E_\nu' \cap F_\nu\}P\{E_\nu'|F_\nu\} \\ &\quad + P\{E_s'|\overline{E_\nu'} \cap F_\nu\}P\{\overline{E_\nu'}|F_\nu\}. \end{aligned} \tag{C1}$$

Now, using the assumption that the up and down times follow the same distribution, $P\{E_s'|E_\nu' \cap F_\nu\} = p_i^*(s,\nu)$ and $P\{E_s'|\overline{E_\nu'} \cap F_\nu\} = 1 - p_i^*(s,\nu)$. Also observe that $P\{\overline{E_\nu'}|F_\nu\} = 1 - P\{E_\nu'|F_\nu\}$. So it only remains to compute

$$\tilde{p}_i := P\{E_\nu'|F_\nu\}, \tag{C2}$$

the probability for an edge to be available at some time, knowing a jump was performed through a competing edge at that time. This would yield the final expression

$$p_i^\dagger(s,\nu) = (2\tilde{p}_i - 1)p_i^*(s,\nu) - \tilde{p}_i + 1. \tag{C3}$$

Let H_ν be the event that the jump at time ν happened after the walker was trapped. Recall that, per (57), we have $P\{H_\nu\} = (1-p)^{|V_i|} = \tilde{q}_i$. Using again the law of total probabilities,

$$\begin{aligned} \tilde{p}_i = &\underbrace{P\{E_\nu'|F_\nu \cap H_\nu\}}_{=0} P\{H_\nu|F_\nu\} \\ &+ P\{E_\nu'|F_\nu \cap \overline{H_\nu}\} \underbrace{P\{\overline{H_\nu}|F_\nu\}}_{=1-\tilde{q}_i}. \end{aligned} \tag{C4}$$

In the second term,

$$P\{E_\nu'|F_\nu \cap \overline{H_\nu}\} = \frac{P\{E_\nu' \cap F_\nu \cap \overline{H_\nu}\}}{P\{F_\nu \cap \overline{H_\nu}\}}, \tag{C5}$$

where the denominator is decomposed as

$$\begin{aligned} P\{F_\nu \cap \overline{H_\nu}\} &= P\{F_\nu \cap \overline{H_\nu}|E_\nu'\}P\{E_\nu'\} \\ &\quad + P\{F_\nu \cap \overline{H_\nu}|\overline{E_\nu'}\}P\{\overline{E_\nu'}\} \end{aligned} \tag{C6}$$

with $P\{E_\nu'\} = p = 1 - P\{\overline{E_\nu'}\}$. Moreover, let $E_\nu^{(k)}$ be the event that k out of $|V_i| - 2$ out neighbors of node i are reachable at time ν, so that

$$\begin{aligned} P\{F_\nu \cap \overline{H_\nu}|E_\nu'\} &= P\{F_\nu|E_\nu'\} \\ &= \sum_{k=0}^{|V_i|-2} P\{F_\nu|E_\nu^{(k)} \cap E_\nu'\}P\{E_\nu^{(k)}|E_\nu'\} \\ &= \sum_{k=0}^{|V_i|-2} p\frac{1}{k+2} \times \binom{|V_i|-2}{k} p^k(1-p)^{|V_i|-2-k} \\ &= \sum_{k=0}^{|V_i|-2} \binom{|V_i|-2}{k} \frac{1}{k+2} p^{k+1}(1-p)^{|V_i|-2-k}. \end{aligned} \tag{C7}$$

Using the same identity that allowed us to obtain (62),

$$\sum_{k=1}^{n} \binom{n-1}{k-1} \frac{1}{k} p^k(1-p)^{n-k} = \frac{1-(1-p)^n}{n}, \quad n \geqslant 1, \tag{C8}$$

one eventually finds that the right-hand side of (C7) reads

$$P\{F_\nu \cap \overline{H_\nu}|E_\nu'\} = \frac{|V_i|p + (1-p)^{|V_i|-1}}{|V_i|(|V_i|-1)p}, \quad |V_i| \geqslant 2. \tag{C9}$$

Similarly, for the remaining factor of (C6) we have

$$\begin{aligned} &P\{F_\nu \cap \overline{H_\nu}|\overline{E_\nu'}\} \\ &= \sum_{k=0}^{|V_i|-2} P\{F_\nu \cap \overline{H_\nu}|E_\nu^{(k)} \cap E_\nu'\}P\{E_\nu^{(k)}|E_\nu'\} \\ &= \underbrace{P\{F_\nu \cap \overline{H_\nu}|E_\nu^{(0)} \cap \overline{E_\nu'}\}}_{=p} \times \underbrace{P\{E_\nu^{(0)}|\overline{E_\nu'}\}}_{=(1-p)^{|V_i|-2}} \\ &\quad + \sum_{k=1}^{|V_i|-2} \underbrace{P\{F_\nu \cap \overline{H_\nu}|E_\nu^{(k)} \cap \overline{E_\nu'}\}}_{=1/(k+1)p} \times \underbrace{P\{E_\nu^{(k)}|\overline{E_\nu'}\}}_{=\binom{|V_i|-2}{k}p^k(1-p)^{|V_i|-2}} \\ &= \sum_{k=0}^{|V_i|-2} \binom{|V_i|-2}{k} \frac{1}{k+1} p^{k+1}(1-p)^{|V_i|-2-k}, \end{aligned} \tag{C10}$$

and relying again on (C8),

$$P\{F_\nu \cap \overline{H_\nu}|\overline{E_\nu'}\} = \frac{1-(1-p)^{|V_i|-1}}{|V_i|-1}, \quad |V_i| \geqslant 2. \tag{C11}$$

Inserting (C9) and (C11) in Eq. (C6) leads to writing (C5) as

$$P\{E_\nu'|F_\nu \cap \overline{H_\nu}\} = \frac{|V_i|p + (1-p)^{|V_i|} - 1}{(1-|V_i|)[(1-p)^{|V_i|} - 1]}, \tag{C12}$$

and eventually (C2) becomes

$$\tilde{p}_i = \frac{|V_i|p + (1-p)^{|V_i|} - 1}{|V_i| - 1}, \quad |V_i| \geqslant 2. \tag{C13}$$

The expression of $p_i^\dagger(s,\nu)$ results from inserting (C13) into (C3).

[1] R. Balescu, *Statistical Dynamics: Matter out of Equilibrium* (Imperial College Press, London, 1997).

[2] D. ben Avraham and S. Havlin, *Diffusion and Reactions in Fractals and Disordered Systems* (Cambridge University Press, Cambridge, UK, 2000).

[3] J. Klafter and I. M. Sokolov, *First Steps in Random Walks: From Tools to Applications* (Oxford University Press, Oxford, 2011).

[4] S. Fedotov, Non-markovian random walks and nonlinear reactions: subdiffusion and propagating fronts, Phys. Rev. E **81**, 011117 (2010).

[5] C. N. Angstmann, I. C. Donnelly, B. I. Henry, and T. A. M. Langlands, Continuous-time random walks on networks with vertex-and time-dependent forcing, Phys. Rev. E **88**, 022811 (2013).

[6] C. N. Angstmann, I. C. Donnelly, and B. I. Henry, Continuous time random walks with reactions forcing and trapping, Math. Modell. Nat. Phenom. **8**, 17 (2013).

[7] C. N. Angstmann, I. C. Donnelly, and B. I. Henry, Pattern formation on networks with reactions: A continuous-time random-walk approach, Phys. Rev. E **87**, 032804 (2013).

[8] R. Kutner and J. Masoliver, The continuous time random walk, still trendy: fifty-year history, state of art and outlook, Eur. Phys. J. B **90**, 50 (2017).

[9] N. Masuda, M. A. Porter, and R. Lambiotte, Random walks and diffusion on networks, Phys. Rep. **716-717**, 1 (2017).

[10] S. Brin and L. Page, Anatomy of a large-scale hypertextual web search engine, in *Proceedings of the Seventh International World Wide Web Conference* (Elsevier Science, Amsterdam, 1998), pp. 107–117.

[11] M. Rosvall and C. T. Bergstrom, Maps of random walks on complex networks reveal community structure, Proc. Natl. Acad. Sci. USA **105**, 1118 (2008).

[12] J. C. Delvenne, S. N. Yaliraki, and M. Barahona, Stability of graph communities across time scales, Proc. Natl. Acad. Sci. USA **107**, 12755 (2010).

[13] R. Lambiotte, J. C. Delvenne, and M. Barahona, Random walks, Markov processes and the multiscale modular organization of complex networks, IEEE Trans. Netw. Sci. Eng. **1**, 76 (2014).

[14] L. Lovász, *Combinatorics, Paul Erdös is Eighty: 2*, Bolyai Society mathematical studies (János Bolyai Math. Soc., Budapest, Hungary, 1996).

[15] P. Holme and J. Saramäki, *Temporal Networks* (Springer-Verlag, Berlin, 2013).

[16] P. Holme, Modern temporal network theory: A colloquium, Eur. Phys. J. B **88**, 1 (2015).

[17] N. Masuda and R. Lambiotte, *A Guide to Temporal Networks* (World Scientific, London, 2016).

[18] M. Karsai, M. Kivelä, R. K. Pan, K. Kaski, J. Kertész, A.-L. Barabási, and J. Saramäki, Small but slow world: How network topology and burstiness slow down spreading, Phys. Rev. E **83**, 025102 (2011).

[19] M. Starnini, A. Baronchelli, A. Barrat, and R. Pastor-Satorras, Random walks on temporal networks, Phys. Rev. E **85**, 056115 (2012).

[20] N. Perra, A. Baronchelli, D. Mocanu, B. Gonçalves, R. Pastor-Satorras, and A. Vespignani, Random Walks and Search in Time-Varying Networks, Phys. Rev. Lett. **109**, 238701 (2012).

[21] J.-C. Delvenne, R. Lambiotte, and L. E. C. Rocha, Diffusion on networked systems is a question of time or structure, Nat. Commun. **6**, 7366 (2015).

[22] T. Hoffmann, M. A. Porter, and R. Lambiotte, Generalized master equations for non-poisson dynamics on networks, Phys. Rev. E **86**, 046102 (2012).

[23] L. Speidel, R. Lambiotte, K. Aihara, and N. Masuda, Steady state and mean recurrence time for random walks on stochastic temporal networks, Phys. Rev. E **91**, 012806 (2015).

[24] M. Gueuning, R. Lambiotte, and J.-C. Delvenne, Backtracking and mixing rate of diffusion on uncorrelated temporal networks, Entropy **19**, 542 (2017).

[25] I. Scholtes, N. Wider, R. Pfitzner, A. Garas, C. J. Tessone, and F. Schweitzer, Causality-driven slow-down and speed-up of diffusion in non-markovian temporal networks, Nat. Commun. **5**, 5024 (2014).

[26] R. Lambiotte, M. Rosvall, and I. Scholtes, Understanding complex systems: From networks to optimal higher-order models, arXiv:1806.05977.

[27] L. Gauvin, A. Panisson, C. Cattuto, and A. Barrat, Activity clocks: spreading dynamics on temporal networks of human contact, Sci. Rep. **3**, 3099 (2013).

[28] K. Zhao, M. Karsai, and G. Bianconi, Entropy of dynamical social networks, PloS one **6**, e28116 (2011).

[29] A. Scherrer, P. Borgnat, E. Fleury, J.-L. Guillaume, and C. Robardet, Description and simulation of dynamic mobility networks, Comput. Networks **52**, 2842 (2008).

[30] V. Sekara, A. Stopczynski, and S. Lehmann, Fundamental structures of dynamic social networks, Proc. Natl. Acad. Sci. USA **113**, 9977 (2016).

[31] D. J. Stilwell, E. M. Bollt, and D. Gray Roberson, Sufficient conditions for fast switching synchronization in time-varying network topologies, SIAM J. Appl. Dyn. Syst. **5**, 140 (2006).

[32] N. Masuda, K. Klemm, and V. M. Eguíluz, Temporal Networks: Slowing Down Diffusion by Long Lasting Interactions, Phys. Rev. Lett. **111**, 188701 (2013).

[33] J. Petit, B. Lauwens, D. Fanelli, and T. Carletti, Theory of Turing Patterns on Time Varying Networks, Phys. Rev. Lett. **119**, 148301 (2017).

[34] D. Figueiredo, P. Nain, B. Ribeiro, E. de Souza e Silva, and D. Towsley, Characterizing continuous time random walks on time varying graphs, in *ACM SIGMETRICS Performance Evaluation Review* (ACM, London, 2012), Vol. 40, pp 307–318.

[35] S. Melnik, A. Hackett, M. A. Porter, P. J. Mucha, and J. P. Gleeson, The unreasonable effectiveness of tree-based theory for networks with clustering, Phys. Rev. E **83**, 036112 (2011).

[36] L. M. Delves and J. L. Mohamed, *Computational Methods for Integral Equations* (Cambridge University Press, Cambridge, UK, 1985).

[37] H. Jasiulewicz and W. Kordecki, Convolutions of erlang and of pascal distributions with applications to reliability, Demonstratio Math. **36**, 231 (2003).

[38] A.-L. Barabasi, The origin of bursts and heavy tails in human dynamics, Nature (London) **435**, 207 (2005).

[39] C. Cattuto, W. Van den Broeck, A. Barrat, V. Colizza, J.-F. Pinton, and A. Vespignani, Dynamics of person-to-person interactions from distributed rfid sensor networks, PloS One **5**, e11596 (2010).

[40] M. Salathé, M. Kazandjieva, J. W. Lee, P. Levis, M. W. Feldman, and J. H. Jones, A high-resolution human contact network for infectious disease transmission, Proc. Natl. Acad. Sci. USA **107**, 22020 (2010).